J. Fluid Mech. (1989), *vol.* 203, *pp.* 199–214
Printed in Great Britain

The growth and collapse of cavitation bubbles near composite surfaces

By A. SHIMA,[1] Y. TOMITA,[1] D. C. GIBSON[2] AND J. R. BLAKE[3]

[1] Institute of High Speed Mechanics, Tohoku University, Sendai, Japan

[2] CSIRO Division of Construction Engineering, Highett, Victoria, 3190 Australia

[3] Department of Mathematics, The University of Wollongong, Wollongong, New South Wales, 2500 Australia

(Received 26 February 1988 and in revised form 14 November 1988)

An experimental study has been made of the growth and collapse of a bubble near a composite surface consisting of two viscoelastic materials. The migratory characteristics of the bubble are examined by means of streak photography. The bubble migration depends not only on the properties of the composite surface but also on bubble size and distance from the surface. Both the surface stiffness and surface inertia are considered to be effective parameters contributing to the bubble migration: the former seeming to be a particularly important factor. The state of neutral bubble collapse, with no migration towards or away from a surface, can be made to occur with an appropriate combination of the surface stiffness and inertia.

1. Introduction

Cavitation damage is one of the most serious problems in modern hydraulic machinery operating at high speeds. Extensive studies of the mechanism of cavitation damage show that a local high pressure produced in the final stage of the bubble collapse is primarily responsible for the damage (e.g. Knapp, Daily & Hammitt 1970). Recently, Tomita & Shima (1986) conducted a detailed experimental study which clarified the mechanisms of impulsive pressure generation and damage pit formation caused by the collapse of a bubble near a solid boundary. They demonstrated that the motion of a bubble, when located very close to the boundary, influences the impulsive pressure generation and hence damage. In particular, it was concluded that the impulsive pressure causing plastic deformation of material was closely related, directly or indirectly, to the behaviour of a liquid jet. In particular, the damage pit caused by the bubble–shock wave interaction, which must be an important mechanism in producing a local high pressure and causing damage to material, essentially resulted from the impact pressure from a liquid microjet.

In general, bubble motion is influenced by the properties of neighbouring surfaces. For example, a rigid wall attracts a bubble during the later stage of collapse, while a free surface repels it (Cole 1948). The idea of a deformable coating to protect a rigid wall originates from an understanding of the migratory characteristics of a bubble near a free surface. This is regarded as one of the potentially useful methods of preventing cavitation damage to surfaces. Rheingans (1950) carried out an experimental investigation, using a vibratory-type accelerated cavitation machine, for the purpose of reducing cavitation damage, and examined the effect of using a coating made of various types of elastic material as well as the relative resistance to pitting of various metal materials. However, he presented no observations of the actual bubble motion.

Gibson (1986) conducted experiments on single bubbles near a compliant boundary. He observed the motion of a spark-induced bubble near a flexible boundary, finding that the bubble collapses and moves away from the surface with a liquid jet being formed by involution of the bubble in the direction of translation (i.e. away from the flexible boundary). These ideas have been developed further in a series of papers by Blake and Gibson (Gibson & Blake 1980, 1982; Blake & Gibson 1981, 1987; Blake 1987). A composite surface consisting of a rubber sheet and an air-filled porous foam backing seems to be an efficient rigid surface coating because the porous foam has a good cushioning effect from the impacts caused by bubble collapse. Gibson & Blake (1982) considered a lumped-parameter description for a deformable surface and proposed a parametric representation of surface interia and stiffness. This proposition yielded a diagram indicating the parameter space for a compliant surface that would repel cavitation bubbles and hence direct the high-speed liquid jet away from the boundary. They also indicated a region on the diagram which they described as 'worth exploring further'. This region was expected to include an optimum deformable surface which would suppress the large impulsive pressures generated by bubble collapse, without being overcompliant. The present joint work was commenced to develop surface coating materials that would effectively reduce the impulsive pressure.

In the following sections we describe an experimental study of the collapse of bubbles near composite surfaces, noting especially the direction of bubble migration. As a result, we show that neutral bubble collapse can occur when some composite surfaces are used. We also show that bubble migration depends not only on the properties of a boundary surface but also on the location and size of the bubble.

2. Experimental apparatus and methods

A schematic diagram of the experimental set-up is shown in figure 1. A vapour bubble is generated by means of an electric spark discharge in tap water at atmospheric pressure and room temperature in a stainless-steel bubble chamber (240 mm × 240 mm × 300 mm). Two different maximum bubble sizes were examined, one corresponding to $R_{\max} = 3.5$ mm, which corresponds to previous experiments on a bubble near a rigid wall (Shima *et al.* 1981, 1983; Tomita & Shima 1986); the other corresponding to $R_{\max} = 5.0$ mm. The bubble size could be determined from a relationship between the input spark energy and maximum bubble radius, which was obtained experimentally by means of streak photography. Tap water at 292.2 ± 3 K was introduced at the base of the chamber to prevent the formation of air bubbles on the test surface.

The optical system is also described in figure 1. Using this system the simultaneous records taken from two directions at right angles are available. The main optical line was provided for streak photography by an Imacon high-speed camera (John Hadland 790), with an He–Ne laser as a light source. A slit width of 0.5 mm was provided at the observation window perpendicular to the test surface. The instantaneous picture was taken with a ruby laser pulse of 20 ns duration and 1.2 J total power as the light source. The timing for photographing was controlled by a delay circuit and an elapsed time from the bubble creation, which corresponds to the difference between the signals obtained from the photocell PC and the photodiode PD, was indicated on a digital counter. In this optical line, F_1 is a filter which bandpasses a wavelength of 694.3 nm, that of the laser. An optical image taken by the shadowgraph method was focused onto the focal plate FP. A signal, generated

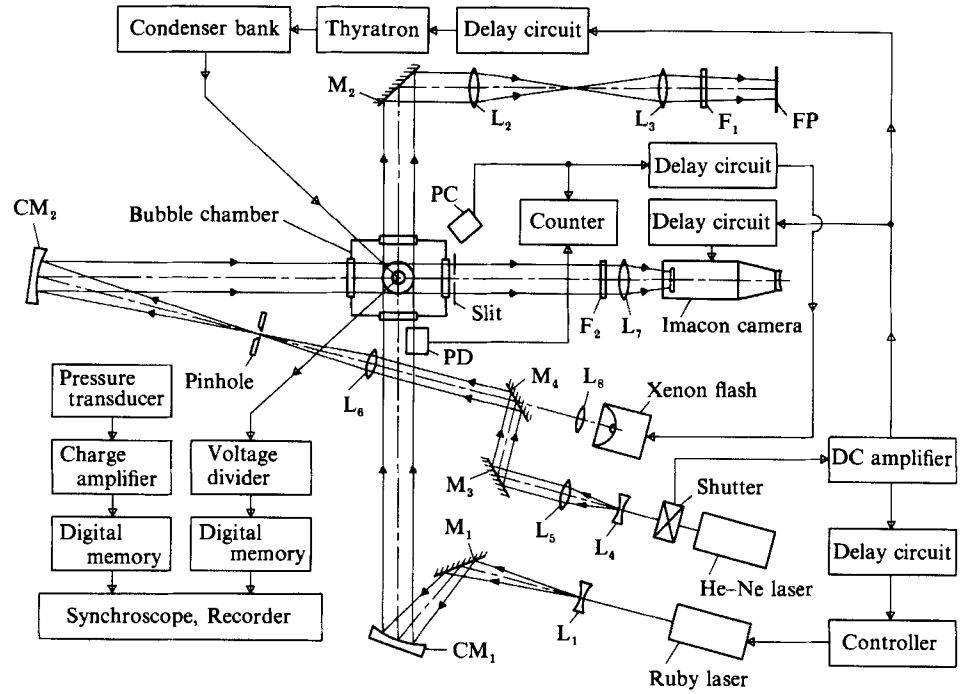

FIGURE 1. Schematic diagram of the experimental set-up.

when the shutter was opened, triggered the DC amplifier which produced instantaneously three signals for creating a bubble and observing its behaviour. To capture the detail of the bubble behaviour, especially the neutral bubble collapse, high-speed photography was used. The system employed a Xenon microflash of about 200 μs with a diffuser as back lighting.

Figure 2 shows a schematic view of the test section. The surface under test is a composite one, of 40 mm diameter, consisting of a foam rubber backing of thickness t_F mm and a nitrile rubber (NBR) sheet of thickness t_R mm. The raw material of the foam rubber is a urethan rubber, a synthetic rubber. The gas phase forms 98% of the foam rubber by volume. The sheet is made from another synthetic rubber, NBR, a copolymer consisting of butadiene and acrylonitrile. The hardness of the two rubbers was measured from hardness-testing Type A (established in the Japanese Industrial Standard) to be 80 for the NBR and 70 for the urethan rubber. The Young's modulus of the NBR was determined as 95.6 kPa with 1% strain. The density of the urethan rubber is 1.20 g/cm^3, that of the foam rubber, ρ_F, is 0.024 g/cm^3 and ρ_R is 1.39 g/cm^3 for the NBR. These two untensioned rubbers, the NBR and the foam rubber, were glued to each other and attached to a brass plate rigid wall as shown in the figure by hatching. The test surface was lowered down onto the water free surface from above, so that the surface of the rubber sheet was in contact with water everywhere, but the foam rubber backing remained gas filled. The thickness of the foam rubber ranged up to 20 mm, and that of the NBR from 0.3 mm to 5 mm. When using a thin NBR sheet, a 5 μm thick polyvinylidene chloride film was used to cover the composite material in order to avoid the permeation of water into the porous foam medium. Although the real situation must be further complicated, the simplest dynamic model for a viscoelastic material like the composite surface under test can be expressed by a

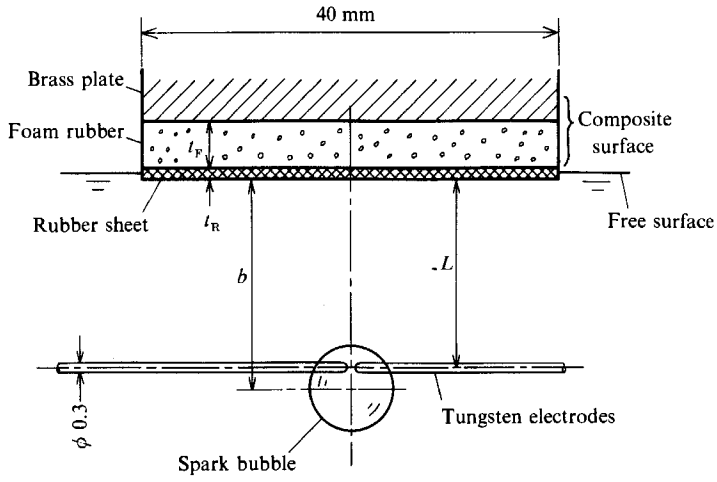

FIGURE 2. Schematic view of the test section.

system consisting of a mass, a spring and a dashpot. Gibson & Blake (1982) applied a one-dimensional oscillating system to a deformable surface and evaluated the boundary characteristics by using effective parameters such as the dimensionless surface inertia m^* and surface stiffness k^*, but excluding damping, which are defined as follows:

$$m^* = \frac{m}{\rho_\ell R_{\max}^3}, \tag{1}$$

$$k^* = \frac{k}{(p_\infty - p_c) R_{\max}} \tag{2}$$

where p_∞ is the pressure in the liquid infinity, p_c the saturation vapour pressure of the liquid, ρ_ℓ the density of the liquid and $R_{\max}$ the maximum bubble radius. Further, k is a spring constant of the composite surface and m is a partial mass of it corresponding to the maximum bubble diameter. Equation (1) can be rewritten as follows:

$$m^* = \frac{\pi(\rho_R t_R + \rho_F t_F)}{\rho_\ell R_{\max}}. \tag{3}$$

The values of k were first determined by pressing circular weights with the same diameter as those of the composite surfaces into them and measuring the initial slope of the load-terminal displacement curve. Figure 3 shows the measured spring constant k against the thickness t_F of the foam rubber, where the laboratory temperature was 292.9 ± 2 K. As t_F increases, k becomes almost constant and independent of t_R. In this case, a representative value is 3.2 kg/cm (i.e. $k^* = 9.0$ when $R_{\max} = 3.5$ mm and $k^* = 6.3$ when $R_{\max} = 5.0$ mm) which is slightly larger than the value $k = 3.0$ kg/cm for the foam rubber alone. In the region $t_F < 5$ mm, on the other hand, k abruptly increases with decreasing t_F as the foam thickness and rigid surface backing assume greater importance even for small perturbations. For the limiting case where t_F is zero, i.e. NBR rubber alone, the value $k = 8.3$ kg/cm was obtained when t_R equals 5 mm. In the real situation of the bubble motion, however, it may be true that an impulsive pressure caused by the bubble collapse locally impacts on a composite surface as spherical load, not cylindrical one with the large diameter of 40 mm. Keeping $t_F = 20$ mm, therefore, the values of k were next examined by press-

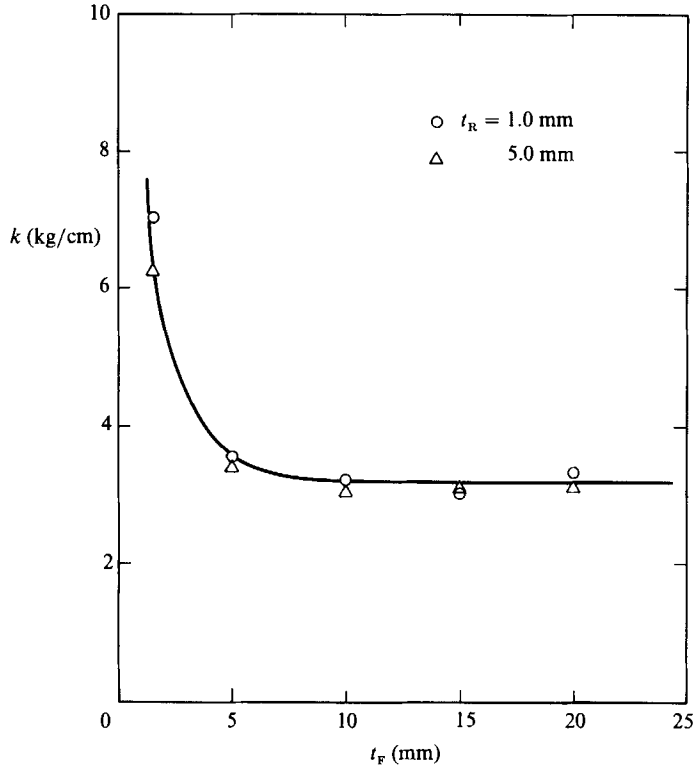

FIGURE 3. Spring constant of composite materials determined from the relationship between cylindrical load and displacement.

ing spherical loads with diameter less than 10 mm, which corresponds to the bigger of the maximum bubble sizes under investigation, into the test surfaces, where the laboratory temperature was 290.7 ± 2 K. The results are shown in figure 4, where a dashed line is an averaged one for the cylindrical-load case obtained already in figure 3. Open squares and triangles correspond to the results obtained for the 20 mm thick foam rubber and one of the Gibson & Blake (1982) materials, consisting of a 1.1 mm thick untensioned natural rubber covering sheet of density 0.94 g/cm^3, and a 7 mm thick open-cell foam rubber with spring constant 0.25 kg/cm. It is clearly seen that the spring constant k varies with mass m_0 of the composite materials depending on the thickness of NBR.

3. Results and discussion

Streak photography is particularly valuable when examining the migratory behaviour of a bubble, provided the slit is set perpendicular to the boundary surface. So, we can see the trajectory of the top and bottom of the bubble surface with the lapse of time. This kind of photographic method clearly indicates whether a bubble is attracted to or repelled by a boundary. Figure 5 is a typical example of a streak picture, with a sketch for explanation on the left showing a relatively small bubble pulsating in an infinite volume of water. The bubble remains almost spherical during the first growth and collapse period. Thereafter, it oscillates several times, gradually rising upward owing to the effect of buoyancy.

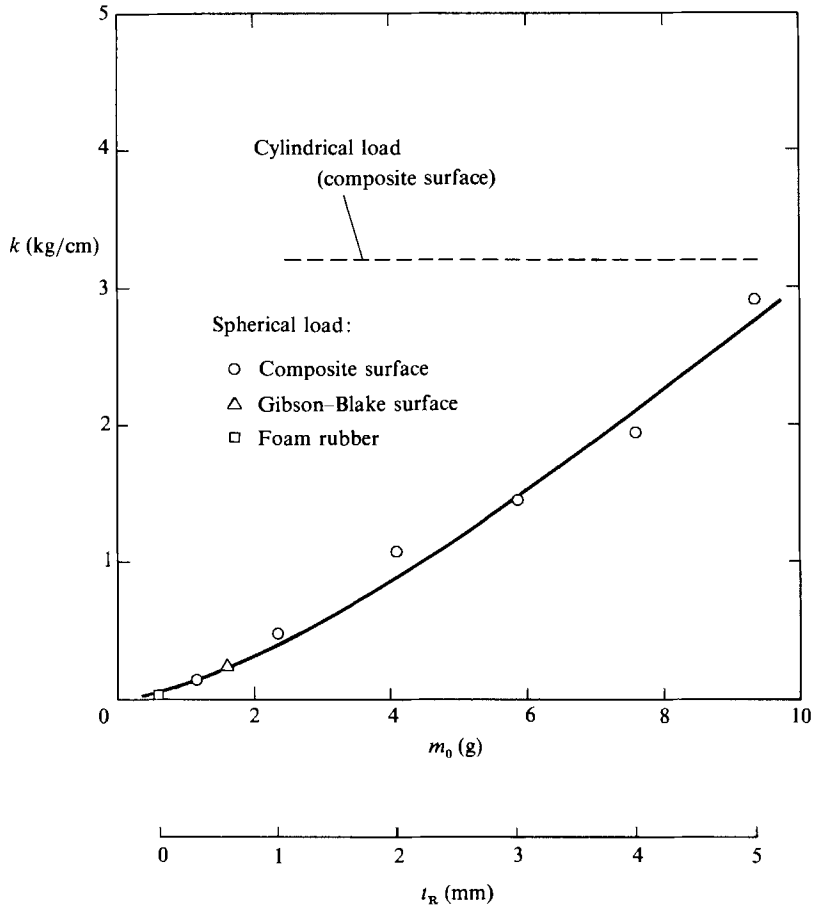

FIGURE 4. Spring constant of various materials determined from the relationship between spherical load and displacement at $t_F = 20$ mm.

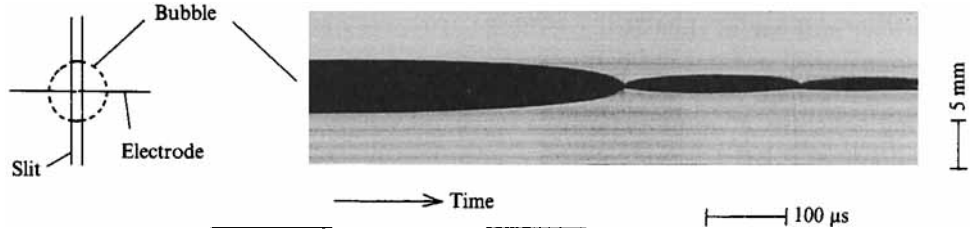

FIGURE 5. Typical example of a streak picture of a bubble in an infinite volume of water ($L \to \infty$).

Using this method, we first examined the effects of changing the thickness t_F of the rubber backing of a composite surface. Figure 6 shows the $b_{R_{min}}/L - t_F$ curves obtained for various thickness of NBR sheet, where $b_{R_{min}}$ is the position of the bubble centre at its minimum size (after collapse), and L the distance between the electrode and the boundary, as defined in figure 2. The results were obtained for the case of $L/R_{max} = 1.14$ ($= \gamma$ in Gibson & Blake 1982), where a bubble acts on a rigid surface most intensely. It is clearly seen that the migratory behaviour of a bubble is strongly

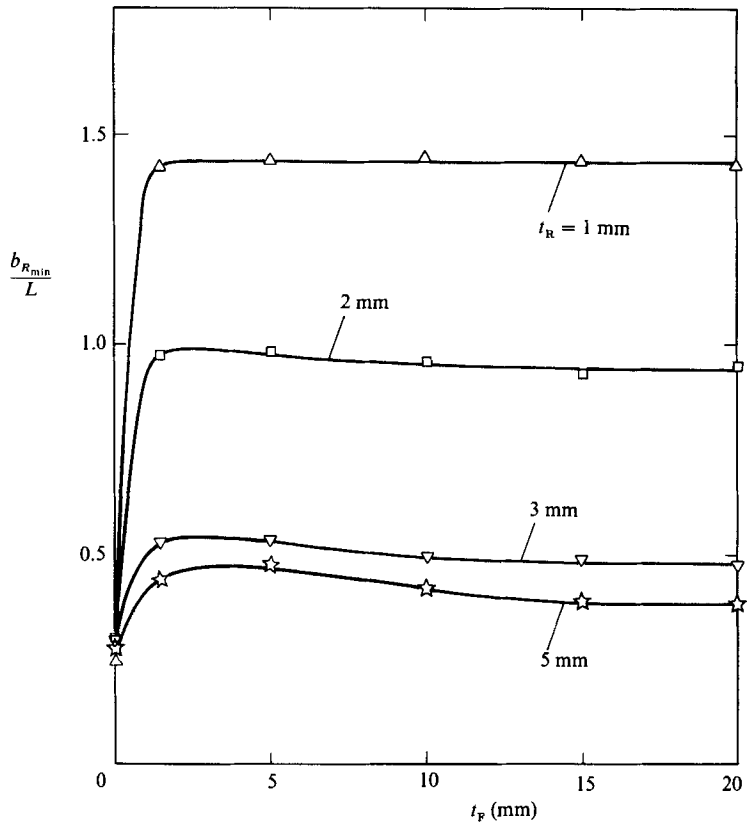

FIGURE 6. Effect of the thickness t_R on the $b_{R_{min}}/L - t_F$ curve (R_{max} = 3.5 mm, L/R_{max} = 1.14; p_∞ = 101.5 kPa, T_∞ = 292.2 K).

affected by the presence of low-density foam rubber, especially when the NBR is thinner than the foam rubber. In this figure, the results for $t_F = 0$ correspond exactly to those for a surface made of only a nitrile rubber sheet attached to a rigid boundary, where the bubbles are all attracted towards the boundary. It is found that a coating of an NBR sheet on a rigid boundary merely reduces the attraction of the bubble towards the boundary; it never 'repels' the bubble. The $b_{R_{min}}/L - t_F$ curves tend to become independent of t_F as it increases. Whereas for $t_R = 2$ mm the bubble behaves almost neutrally because no migration takes place at $b_{R_{min}}/L = 1$, for $t_R = 1$ mm the bubble is repelled by the composite boundary. These results suggest that response of the bubble may be determined not only by t_R, in other words surface inertia m^*, but also by surface stiffness k^*, once a critical value of t_F is exceeded. In all the following experiments we have set t_F to be 20 mm.

Figure 7 shows simultaneous pictures at the first collapse of bubbles near composite surfaces, foam rubber, a rigid wall and a free surface, where the pair of fine black lines appearing clearly on the instantaneous pictures (*b*) are electrodes. The white spot on the streak pictures (*a*) is the ruby laser light scattered from the bubble surface, which identifies exactly the timing of the instantaneous picture, (*b*). In figure 7(v)(*b*), the black line of relatively broad width is the meniscus of water at its interface with the optical window. The impedance of each surface reduces as the picture number increases from (i) to (v). It is clear that the bubble migration is

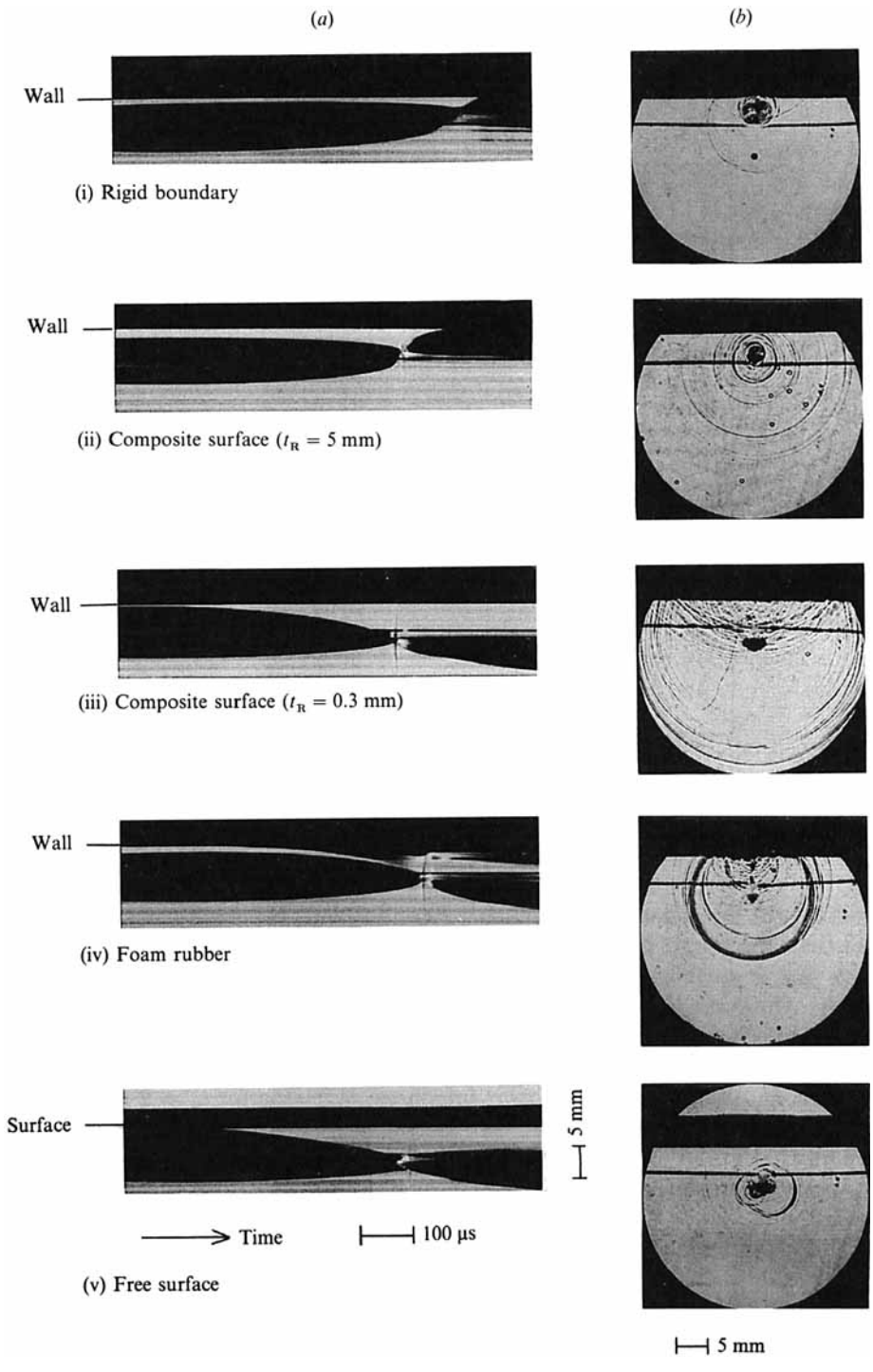

FIGURE 7. Simultaneous records of (*a*) a streak photograph and (*b*) an instantaneous picture at the first collapse of bubbles near various kinds of boundaries (R_{max} = 3.5 mm).

dependent on the physical properties of the boundary. For example, a bubble migrates towards a rigid surface and away from both a free surface and foam rubber. On the other hand, in cases (ii) and (iii) of the composite-surface examples, the bubble motion is in the opposite directions. This suggests the existence of a neutral bubble collapse, where the bubble centroid maintains its initial position with no migration. The only difference between cases (ii) and (iii) is the thickness t_R of the NBR sheet, i.e. surface inertia m^* and stiffness k^*. The different responses of the composite surfaces to the applied force induced by the bubble motion result in a different flow field around the bubble, and finally determine the direction of bubble migration. In the streak picture of case (iv), a black part of the foam rubber surface appears to attach to the bubble surface as the bubble becomes small. Considering that the natural period of motion of the foam rubber can be determined as 2.8 ms, which is much longer than the characteristic lifetime of a relatively small bubble (about 1 ms for $R_{max} = 5$ mm) this must be independent of the resonant response of the foam rubber. In this case, the bubble behaves almost spherically during the first growth and collapse period. This implies that the foam rubber surface was deformed flexibly in response to the bubble motion. So, one explanation of the downward dipping of the black area is that deformation of the foam rubber itself occurs, resulting from the force on its surface produced by the rapid change in momentum of the water flowing between the foam rubber surface and the bubble surface in the collapse process. Alternatively it could be a shadow either of gas bubbles sucked out from the surface of the porous medium or of tiny bubbles generated in the collapse process of the bubble near it (see figure 9). There may be a combination of the two.

The instantaneous pictures, figure 7(*b*), show the situations just before and after the shock wave generation. The comparison between cases (i) and (ii) is especially interesting. A reflected wave can be seen in figure 7(i)(*b*) but not in figure 7(ii)(*b*). The reason may be due to the difference in acoustic impedances of the two surfaces. In general, a rigid wall like the brass plate used here has a very high acoustic impedance, while the value measured for the nitrile rubber is roughly two times that of water. It would appear that the shock wave passes through the rubber interior leaving an extremely weak reflected wave. On the other hand if the rubber is very thin, we can see many waves reflected from the NBR–foam rubber interface as well as the primary shock waves, as shown in figure 7(iii)(*b*). An instantaneous picture of figure 7(iv)(*b*) was taken at about 6 μs after rebound of a bubble. Two kinds of shock waves are visible. The bigger one is radiated directly from the main bubble and the other emanates from a bubble generated during the collapse period of the main bubble. Of course, shock waves are generated not only at the instant of rebound of a bubble but also at bubble initiation. If a viscoelastic surface is extremely light and compliant, it may deform owing to the impact of a shock wave produced at bubble initiation.

Results measured from the streak pictures are plotted in figure 8, where each point is an averaged value of five data points. In this figure the bubble centre at the first minimum bubble size, $b_{R_{min}}$, is determined as a function of the generation point of a bubble L for various t_R, including results for a free surface and a rigid boundary. The condition of $b_{R_{min}}/L > 1$ indicates bubble migration away from the surface, while $b_{R_{min}}/L < 1$ corresponds to bubble attraction towards the surface. No migration takes place at $b_{R_{min}}/L = 1$, which is called the condition of neutral collapse for a bubble. In the same figure, results obtained using one of the Gibson & Blake (1982) materials are illustrated by a dashed line. The $b_{R_{min}}/L - L/R_{max}$ curve using this surface is located near the $t_R = 1$ mm case. It is quite obvious that the composite surface possesses an intermediate characteristic between a free surface and a rigid

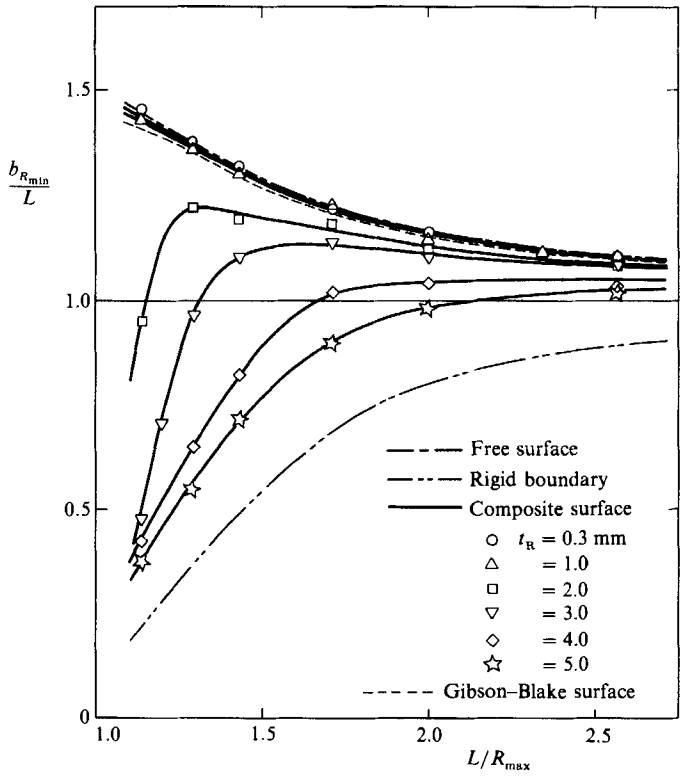

FIGURE 8. $b_{R_{min}}/L - L/R_{max}$ curve (R_{max} = 3.5 mm, p_∞ = 101.5 kPa, T_∞ = 292.2 K).

wall. If t_R becomes small, the subsequent bubble migration tends to be close to that observed for a free surface. On the other hand, if t_R becomes large, migration approaches the result obtained for the rubber surface alone. It is worth noting that, for these experiments, when a bubble pulsates relatively far from a composite surface, it always migrates away from the surface. This means that our attention should be focused on the situation of bubbles located very close to a composite surface.

If t_R is less than 2 mm, then almost all the bubbles located in the region $L/R_{max} > 1$ collapse away from the composite surfaces within the limit of the present work. When a surface is very flexible, an interesting phenomena may occur. Figure 9 is a typical example, showing pictures taken with a framing rate of 100000 frames/s, for three different surfaces, including a separate picture located in the left corner corresponding to the bubble at maximum size. In all cases the bubble moves away from the boundary at its first collapse. Further, we observe many tiny bubbles induced in the rebound process of the bubble motion, for cases (*a*) and (*b*), which is usually called secondary cavitation (Gibson 1968), while they are also generated in the collapse process of a bubble near the Gibson–Blake surface for case (*c*). The domain (m^*, k^*) is (1.7, 1.4) for (*b*) and (1.1, 0.71) for (*c*). The latter case seems to be closely associated with the deformation of the composite surface, which can be easily conjectured from the almost spherical configuration of the bubble at its maximum size. Thereafter the material surface continuously rises upward owing to the inertia effect which competes with tension and gravity, while the bubble begins to collapse. The difference in characteristic timescales between the response of the composite

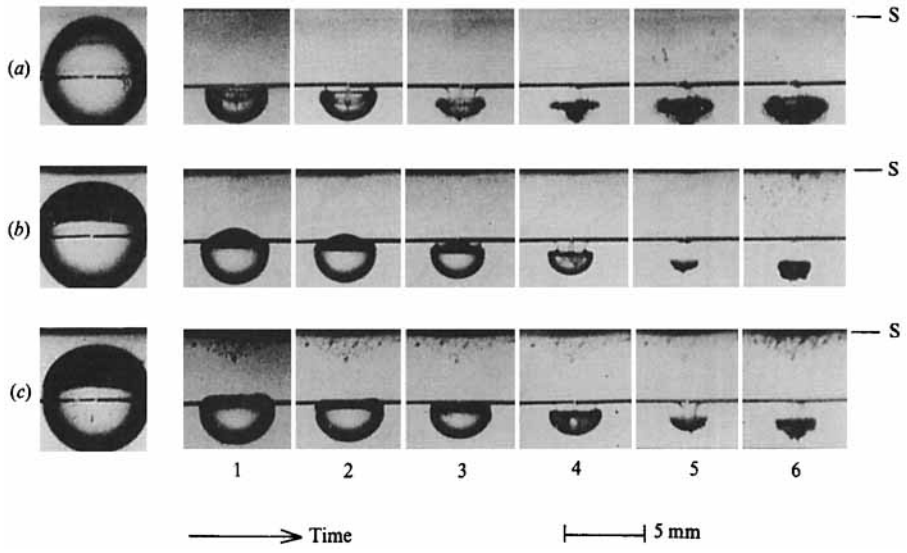

FIGURE 9. Generation of the secondary cavitation: (*a*) free surface, (*b*) composite surface ($t_R = 1.0$ mm), (*c*) Gibson–Blake surface ($R_{max} = 3.5$ mm, $L/R_{max} = 1.14$; S, surface; frame interval = 10 μS).

surface and the bubble motion results in a complicated flow pattern in water existing between the composite surface and the bubble. This must lead to the creation of a number of tiny bubbles, once a critical condition is achieved. The tiny-bubble cluster varies with time according to the pressure fluctuation induced by the motion of the main bubble, which emanates a shock wave into water between the fourth and fifth frames of figure 9(*c*).

Figure 10 indicates the results of $b_{R_{min}}/R_{max}$ versus m^* (or t_R) for various L/R_{max}. A dashed line, $b_{R_{min}} = L$, shows the condition of neutral collapse of bubbles. Each curve tends to approach the value for a free surface for vanishing m^*, while it tends to the constant value for a rubber sheet alone for larger m^*. However, a noticeable effect of the foam rubber on the bubble migration remains even when $t_R = 5$ mm. So, there is a definite difference between the data from the composite surface and from the rubber sheet alone for the same dimensionless surface inertia m^*. It is readily seen that a bubble tends to be attracted to a surface as t_R increases. In other words, a sufficiently thin rubber sheet will be required for repelling a bubble located very close to the composite surface. Figure 11 shows the relationship between $b_{R_{min}}/R_{max}$ and k^* for two values of L/R_{max}. In this figure, open circles and triangles correspond to the data for the composite surfaces and the Gibson–Blake surface, respectively. Also, the data for the rubber sheet alone are plotted with solid circles. The results clearly indicate the important finding that the surface stiffness of the composite material significantly influences the bubble migration. In particular, it is worth noting that $b_{R_{min}}/R_{max}$ can be described as a function of the variable k^* obtained for various kinds of surfaces. The $b_{R_{min}}/R_{max} - k^*$ curve abruptly changes near the condition of $b_{R_{min}} = L$, the neutral bubble collapse. This is a quite different tendency from the $b_{R_{min}}/R_{max} - m^*$ curve. Since stiffness is closely related to vertical displacement, it can be conjectured that the Young's modulus must be one of the most important factors contributing to the bubble migration.

Next we consider the neutral condition of bubble collapse. Figures 12 and 13 are typical examples of the behaviour before and after collapse of a bubble near a

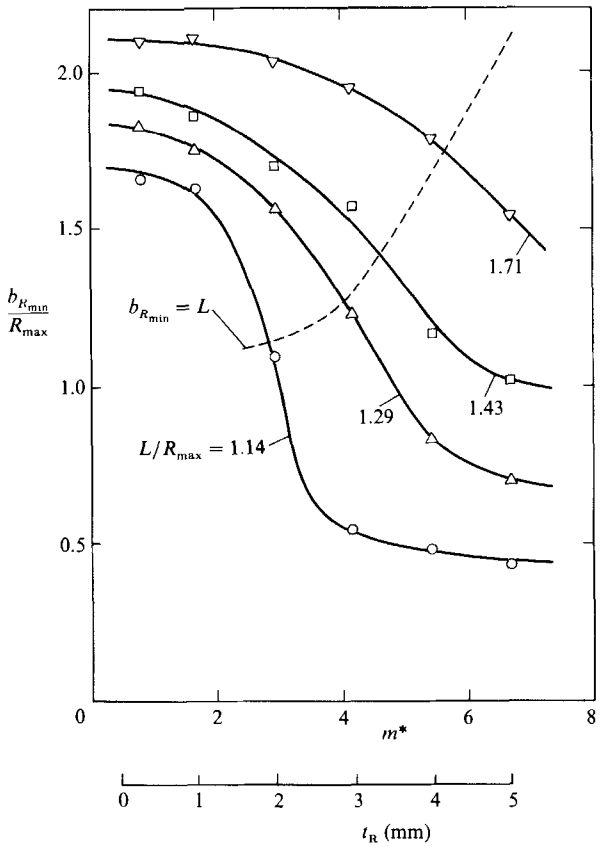

FIGURE 10. Effect of the surface inertia m^* on bubble migration ($R_{max} = 3.5$ mm, $t_F = 20$ mm, $p_\infty = 101.5$ kPa, $T_\infty = 292.2$ K).

composite surface consisting of a 2 mm thick NBR sheet and 20 mm thick foam rubber. A bubble with radius 3.5 mm was generated at a distance $L = 4.0$ mm, i.e. the dimensionless distance L/R_{max} equals 1.14. The results in figure 12 were recorded by means of streak photography, while those in figure 13 were recorded at a framing rate of 100000 frames/s. Since this case is very close to the condition for neutral bubble collapse, the bubble configuration is quite strange. Streak pictures shown in figure 12 are different from each other in their rebound periods. Figure 12(*b*) was obtained for a situation where a slit was located at a slight distance away from centrally between the electrodes. In the final stage of the collapse of a bubble near a composite surface around the neutral condition, the bubble tends to separate into two parts connected by a thin chord. Therefore, light can easily pass around its edges resulting in the splitting phenomenon exhibited in figure 12(*b*). The matter is clarified by the picture sequences shown in figure 13. This kind of bubble shape is very similar to that of a bubble collapsing between two rigid boundaries (Shima & Sato 1980). Apparently, there is no liquid jet towards the boundary; instead a necking phenomenon occurs at the final stage of the collapse (Gibson & Blake 1982). Thereafter each separate part grows in the rebounding period. The condition for neutral collapse of bubbles with maximum radii of 3.5 mm and 5.0 mm near the present composite surfaces is summarized in figure 14, where t_F is 20 mm. The shaded

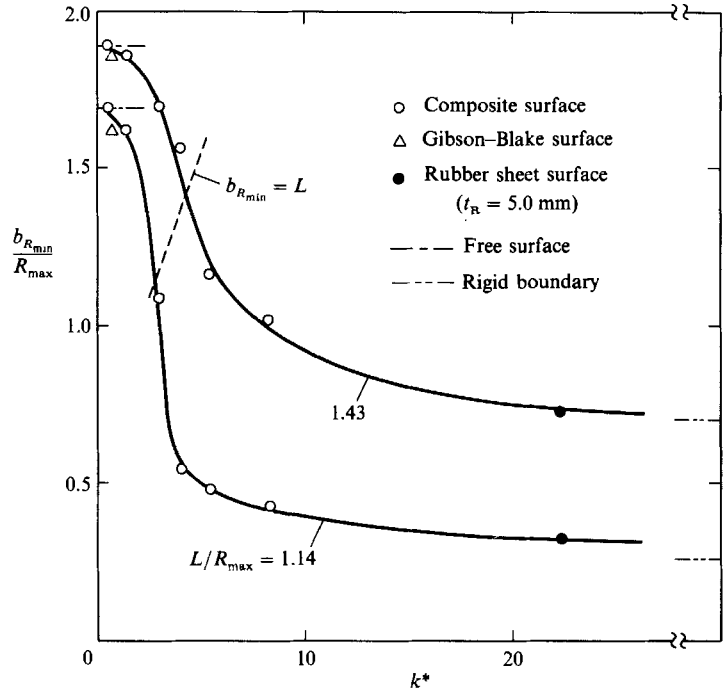

FIGURE 11. Effect of the surface stiffness k^* on bubble migration (R_{max} = 3.5 mm, t_F = 20 mm, p_∞ = 101.5 kPa, T_∞ = 292.2 K).

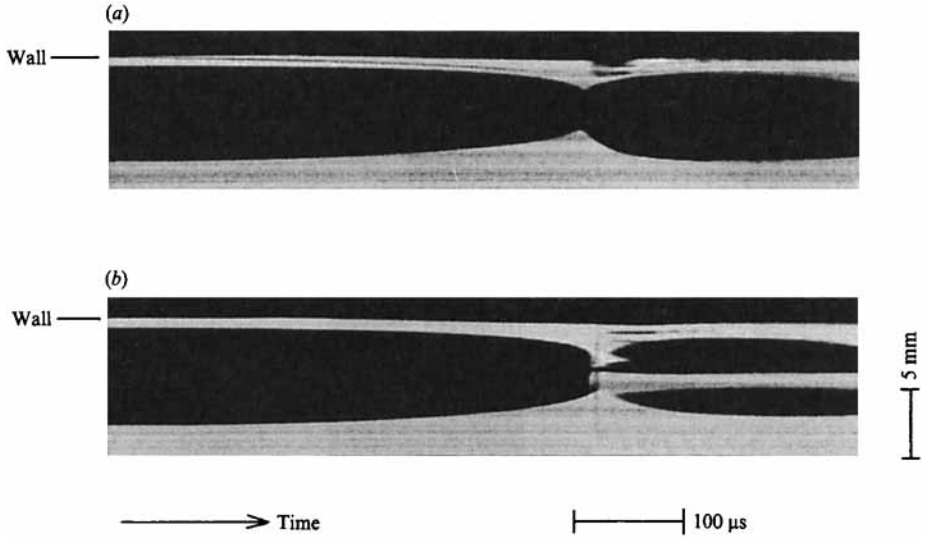

FIGURE 12. Streak pictures of the collapse of a bubble near a composite surface: the situation is very close to neutral bubble collapse. In (*b*) the slit is moved slightly from the central position between two electrodes (R_{max} = 3.5 mm, L/R_{max} = 1.14; t_R = 2 mm, t_F = 20 mm).

portion identifies the repulsive region, where a bubble is completely repelled from the boundary. When the bubble size becomes larger, the limiting curve shifts towards larger t_R. We conclude that bubble migration depends not only on the properties of the boundary surfaces, but also on the bubble conditions such as the size and distance from the surface.

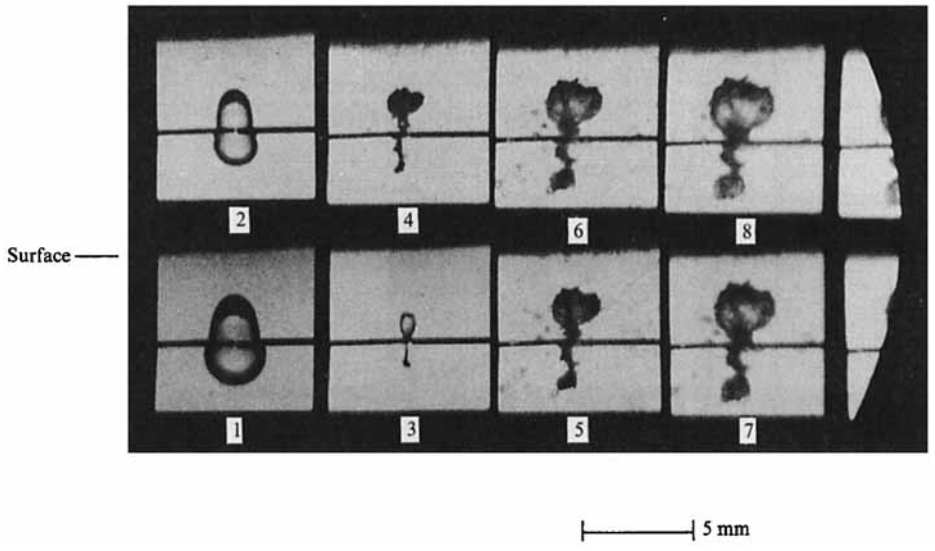

FIGURE 13. Frame-by-frame pictures of the collapse of a bubble near a composite surface: the situation is very close to neutral bubble collapse ($R_{max} = 3.5$ mm, $L/R_{max} = 1.14$; $t_R = 2$ mm, $t_F = 20$ mm; frame interval = 10 μs).

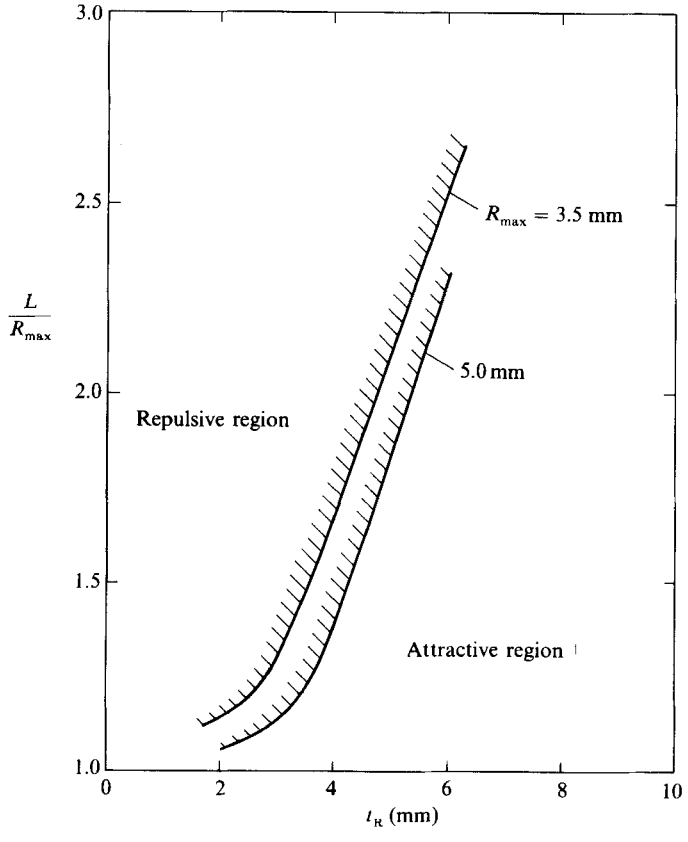

FIGURE 14. Condition of neutral bubble collapse ($p_\infty = 101.5$ kPa, $T_\infty = 292.2$ K).

Bubble migration has previously been discussed in terms of the Kelvin impulse (Blake 1983), which is a valuable concept in determining global characteristics such as bubble migration. Recently, Blake (1987) has theoretically confirmed a part of our experimental evidence concerning the neutral collapse of a bubble near a composite surface: that the limiting curve showing the relation between $L/R_{\max}$ and t_{R} tends to be linear when surface displacement is relatively small.

4. Concluding remarks

An experimental study of the growth and collapse of spark-induced bubbles near composite surfaces, over the region $L/R_{\max} > 1$, has been made. The composite surfaces examined locally have a relative low boundary stiffness, which increases with increasing mass of the composite material. Under this condition, the surface displacements are significantly influenced by the boundary stiffness k^* as well as inertia m^*. The study has shown that bubble migration depends not only on the properties of a boundary surface but also on bubble size and location relative to the surface. The dynamic behaviour of a bubble near a composite surface is influenced by the difference in characteristic timescales between the response of the surface and the bubble motion. Once surface response is permitted, an elastic restoring force from the composite surface can inject stored energy back into the liquid later in the cycle. It is therefore important to know the dynamic response of a composite surface to impulsive forces such as those caused by the growth and collapse of a cavitation bubble. The present work has been focused on the region of $L/R_{\max} > 1$. It is planned to investigate the region for $L/R_{\max} < 1$ using a laser-induced bubble in the near future.

The authors wish to express their thanks to Professor K. Takayama of Tohoku University for his useful suggestions. Assistance received from Mr N. Miura, Mr K. Shoji, Mr K. Izumi, Miss N. Inomata and Miss M. Monma is acknowledged with thanks. Research funding from the Australian Research Grants Committee is also acknowledged.

REFERENCES

BLAKE, J. R. 1983 The Kelvin impulse: applications to bubble dynamics. In *Proc. 8th Australasian Conf. on Hydraulics and Fluid Mechanics, University of Newcastle, New South Wales*, pp. 10B. 1–10B. 4.

BLAKE, J. R. 1987 The Kelvin impulse: application to cavitation bubble dynamics. *Reports of the University of Wollongong, Preprint No.* 21.

BLAKE, J. R. & GIBSON, D. C. 1981 Growth and collapse of a vapour cavity near a free surface. *J. Fluid Mech.* **111**, 123–140.

BLAKE, J. R. & GIBSON, D. C. 1987 Cavitation bubbles near boundaries. *Ann. Rev. Fluid Mech.* **19**, 99–123.

COLE, R. H. 1948 *Underwater Explosions*. Princeton University Press.

GIBSON, D. C. 1968 Cavitation adjacent to plane boundaries. In *Proc. 3rd Australasian Conf. on Hydraulics and Fluid Mechanics, Sydney*, pp. 210–214.

GIBSON, D. C. & BLAKE, J. R. 1980 Growth and collapse of cavitation bubbles near flexible boundaries. In *Proc. 7th Australasian Conf. on Hydraulics and Fluid Mechanics, Brisbane*, pp. 283–286.

GIBSON, D. C. & BLAKE, J. R. 1982 The growth and collapse of bubbles near deformable surfaces. *Appl. Sci. Res.* **38**, 215–224.

KNAPP, R. T., DAILY, J. W. & HAMMITT, F. G. 1970 *Cavitation*. McGraw-Hill.

RHEINGANS, W. J. 1950 Accelerated cavitation research. *Trans. ASME* **72**, 705–719.

SHIMA, A. & SATO, Y. 1980 The behavior of a bubble between narrow parallel plates. *Z. Angew. Math. Phys.* **31**, 691–704.

SHIMA, A., TAKAYAMA, K., TOMITA, Y. & MIURA, N. 1981 An experimental study on effects of solid wall on the motion of bubbles and shock waves in bubble collapse. *Acustica* **48**, 293–301.

SHIMA, A., TAKAYAMA, K., TOMITA, Y. & OHSAWA, N. 1983 Mechanism of impact pressure generation from spark – generated bubble collapse near a wall. *AIAA J.* **21**, 55–59.

TOMITA, Y. & SHIMA, A. 1986 Mechanisms of impulsive pressure generation and damage pit formation by bubble collapse. *J. Fluid Mech.* **169**, 535–564.